Thin Solid Films 636 (2017) 158–163

Contents lists available at ScienceDirect

Thin Solid Films

journal homepage: www.elsevier.com/locate/tsf

Opto-electrical characterisation of In-doped SnS thin films for photovoltaic applications

A. Urbaniak [a,*], M. Pawłowski [a], M. Marzantowicz [a], T. Sall [b], B. Marí [b]

[a] Faculty of Physics, Warsaw University of Technology, Koszykowa 75, PL 00-662 Warszawa, Poland
[b] Insitut de Disseny i Fabricació, Universitat Politècnica de València, Cami de Vera s/n, 46022, Valencia, Spain

ARTICLE INFO

Article history:
Received 12 January 2017
Received in revised form 20 April 2017
Accepted 1 June 2017
Available online 01 June 2017

Keywords:
SnS films
Photovoltaics
Spray pyrolysis
Photoluminescence

ABSTRACT

Spray pyrolised SnS thin films doped with indium were studied using various optical and electrical techniques. Structural analysis shows that all films crystallise in an orthorhombic structure with (111) as a preferential direction, without secondary phases. The doping of SnS layers with indium results in better morphology with increased grain size. Absorption measurements indicate a dominant direct transition with energy decreasing from around 1.7 eV to 1.5 eV with increased indium supply. Apart from the direct transition, an indirect one, of energy of around 1.05 eV, independent of indium doping, was identified. The photoluminescence study revealed two donors to acceptor transitions between two deep defect levels and one shallower one, with an energy of around 90 meV. The observed transitions did not depend significantly on In concentration. The conductivity measurements reveal thermal activation of conductivity with energy decreasing from around 165 meV to 145 meV with increased In content.

1. Introduction

Thin film photovoltaics are nowadays dominated by CdTe- and Cu(In,Ga)Se_2-based technologies [1,2]. However, the supply issues of In, Ga and Te as well as the toxicity and disposal requirements of Cd have stimulated the search for other photovoltaic materials. Therefore, more simple, binary and Earth-abundant compounds like SnS [3], FeS_2 [4] and Cu_2S [5] have recently received interest in the photovoltaic community. SnS has high optical absorption of photons with energies above 1,3 eV [3,6], which is in the range of 1–1.5 eV considered as the bandgap energy boundaries for an optimum absorber in solar cells [7]. SnS shows an intrinsic p-type conductivity due to the formation of tin vacancies V_{Sn} [3,6] with carrier concentrations above 10^{15} cm^{-3} [3]. Despite these promising electrical and optical parameters, the efficiencies of SnS-based solar cells are far from satisfactory, with a record efficiency of 4,36% [8]. Moreover, this record has been achieved using Atomic Layer Deposition, which is not a well scalable technique considering solar cell production beyond the laboratory scale. Here we investigated SnS thin films made by spray pyrolysis [9,10]: a simple, inexpensive and versatile technique suitable for industrial-scale production. In this case, the efficiencies obtained so far are below 2% [3]. This could be due to the intrinsic limitations of the material or due to the lack of proper material growth and device optimisation. One of the most important issues for an absorber material is control of its carrier concentration by either appropriate doping or growth parameters. Theoretical calculations [11] predict that an antisite defect In_{Sn} has low formation energy (around 1 eV) under S-rich growth conditions, and should act as a shallow acceptor introducing holes into material. The defect concentration n_s can be estimated as

$$n_S \approx N_{Sn} \exp\left(\frac{H_S}{k_B T}\right) \quad (1)$$

where N_{Sn} is the concentration of Sn atoms, H_s is the In_{Sn} formation enthalpy k_B is the Boltzmann constant and T is the temperature. Based on the formation enthalpy we can estimate the number of defects at 350 °C, which was the growth temperature to be around $3.4*10^{16}$ cm^{-3}. Even though this defect concentration is too low to be detected by most of the techniques it is a typical value of hole concentrations in semiconductors and can significantly affect its electrical parameters. Here, we prepared In-doped SnS thin films by spray pyrolysis [12,13] and studied their basic optical and electrical properties.

2. Experimental

2.1. Thin film preparation

The SnS films were prepared using an aqueous solution containing tin (II) chloride dehydrate ($SnCl_2 \cdot 2H_2O$) and thiourea ($SC(NH_2)_2$). The

* Corresponding author.
E-mail address: aleksander.urbaniak@if.pw.edu.pl (A. Urbaniak).

http://dx.doi.org/10.1016/j.tsf.2017.06.001
0040-6090/

molarities of both solutes were 0,104 M. Indium chloride ($InCl_3$ 99,999% purity) was directly added to the solution at different concentrations ([In]/[Sn] = 0; 0,03; 0,06, and 0,09). To avoid the milky solution resulting of the dissolution of $SnCl_2 \cdot 2H_2O$ in bi-distilled water, it is required to dissolve the stannous chloride dihydrate with chloride acid (37%) before mixed it in sulfur solution. The solution was sprayed at a 1,5 mL/min rate for 4 min on the glass substrate keeping the constant substrate temperature of 350 °C. The pressure of the carrier gas was 0,7 bar and the distance nozzle-substrate was 25 cm. To avoid growth of Sn_2S_3 and SnS_2 phases, Sn (II) instead of Sn(IV) was used [14]. The SnS growth receipt was adapted from the previous work concerning spray pyrolised SnS thin films [15]. Based on it we estimated the [Sn]/[S] ratio to be close to 1 and the thicknesses of the layers to be around 1 μm. To obtain clean and stain-free substrates, an ultrasonic bath was used, and the substrates were cleaned by acetone, distilled water, ethanol and distilled water.

2.2. Thin film characterisation

The X-Ray Diffraction (XRD) measurements were made using a Rigaku Ultima IV diffractometer at the Bragg-Brentano (θ–2θ) configuration and with Cu:Kα radiation (1,5418 Å). Atomic Force Microscopy (AFM) analysis was carried out using an NT-MDT NTEGRA PRIMA microscope in semi-contact mode. The optical properties, including transmittance and reflectance, were measured using Bentham PVE300 setup in the 300–1800 nm range of light wavelength using a halogen and wolfram light source and Ge and Si photodetectors. The reflectance was measured in the diffused standard. The photoluminescence (PL) was evaluated using the lock-in technique. The samples were excited with 514,5 nm chopped Ar + laser light in the laser power output range from 4 to 500 mW, which corresponds to the excitation density roughly from 100 mW/cm^2 to 12,5 W/cm^2. The PL signal was collected with an iHR550 grating monochromator and detected with a liquid nitrogen-cooled germanium detector. The samples were cooled down to low temperatures in the helium closed-cycle setup and analysed in the 10–100 K temperature range. To perform electrical measurements, Al electrodes were evaporated on SnS film in planar configuration. The conductivity was then measured in a nitrogen-cooled cryostat in the 80–330 K temperature range.

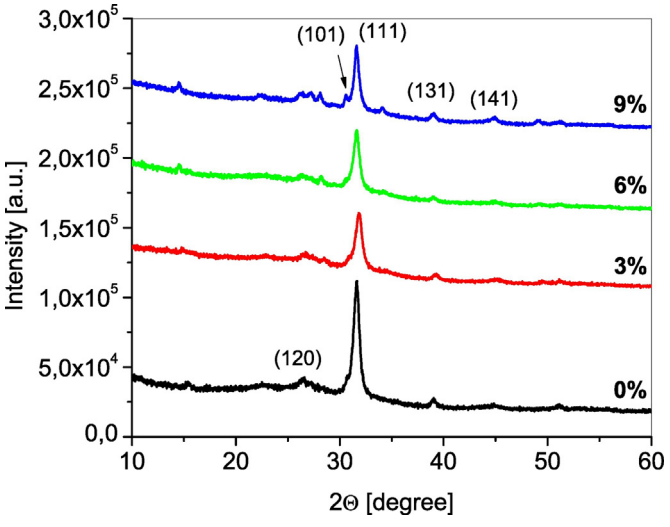

Fig. 1. XRD spectra for SnS samples with different In concentrations in the sprayed solution. Preferential crystallographic directions are also shown.

3. Results and discussion

3.1. XRD analysis and AFM measurements

To investigate the crystalline properties of the synthesised films, XRD measurements were carried out, together with AFM imaging. The diffraction spectra of all four SnS thin films are presented in Fig. 1.

All films are polycrystalline and the XRD peaks are in good agreement with standard data for SnS orthorhombic phase (JCPDS #39-0354) with (111) as the preferential crystallographic direction. The peaks are broad, which indicates high disorder in the material, as well as point into small crystallite sizes. The intensity of the (111) main peak decreases with increasing amount of In. The crystallite size of SnS thin film doped with indium for the main (111) XRD peak can be calculated using the Scherrer formula: $D = k\lambda/\beta\cos\theta$. Here D is the crystalline size, k is a crystallite shape factor being in the range of 0,62–2,08 [16] (k = 0.9 was used), λ = 1,5418 Å is the wavelength of X-ray radiation, β is the full width at half maximum (FWHM) of the Gaussian peak fitted to the data, and θ is the Bragg angle of diffraction. To determine θ and FWHM parameters, we used the X'Pert HighScore software. The calculated crystallite sizes are presented in Table 1. The size of the crystallites in the investigated samples is in the range 116–125 Å, and does not depend significantly on the amount of indium supplied during growth.

Fig. 2 presents AFM images of two investigated SnS thin films – the undoped one and the one with 9% of indium concentration in the solution. The scan area was 8 μm × 8 μm with 512 × 512 resolution. The films have an irregular structure with longitudinal type of grains, which has already been observed in spray pyrolised SnS thin films [10]. The average grain size and the average roughness height are presented in Table 1. The presence of indium during growth generally increases the mean grain size from around 38 nm to around 60 nm as well as the roughness of the film. However, there is no further increase of grain size when more indium is added. The average grain size is also larger than the average crystallite size obtained from XRD. This might be the result of the different physical meaning of the calculated size parameters between the XRD and AFM analyses. The Scherrer equation gives the minimum crystallite size and the analysis of AFM provides the mean grain size. Taking into account that the grains are clearly longitudinal, we might expect higher average grain sizes then the minimum crystallite width. The second reason might be the fact that the grains could actually consist of few smaller crystallites indistinguishable by AFM analysis.

3.2. Absorbance

According to basic semiconductor equations, the absorption coefficient, in the case of direct transitions, is proportional to:

$$\alpha \propto \frac{1}{h\upsilon}\left(h\upsilon - E_g\right)^{1/2} \tag{2}$$

where h is Planck's constant, ν is the frequency of incident photons and E_g is the bandgap energy. In the case of indirect allowed transitions, the absorption coefficient is proportional to:

$$\alpha \propto \frac{1}{h\upsilon}\left(h\upsilon - E_g \pm E_{ph}\right)^2 \tag{3}$$

Table 1
Size of crystallites calculated from XRD spectra and grain parameters calculated based on the AFM images.

sample	crystallite size (Å)	mean grain size (nm)	mean roughness height (nm)
SnS: undoped	125	37,7 ± 3,8	155 ± 27
SnS: In 3%	116	61,0 ± 9,2	193 ± 25
SnS: In 6%	125	62,6 ± 6,8	196 ± 20
SnS: In 9%	119	58,6 ± 6,5	203 ± 38

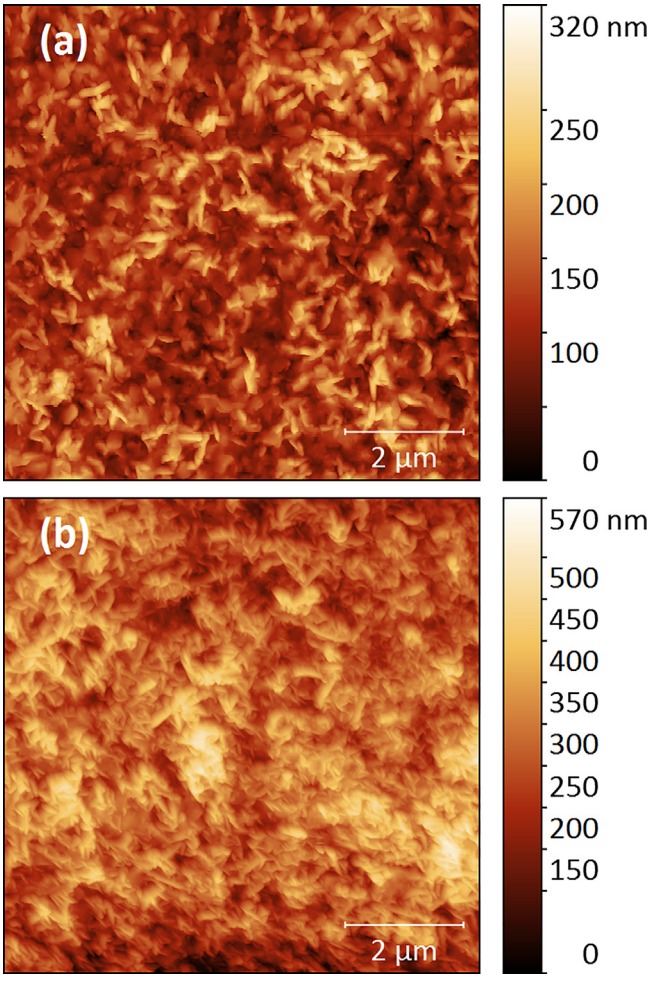

Fig. 2. AFM images of (a) an undoped SnS thin and (b) a SnS thin film with 9% concentration of In in the sprayed solution.

where E_{ph} is the energy of the phonons, the plus sign relates to the phonon absorption and the minus to phonon emission. Thus, the extrapolation of the straight part of either $(\alpha h\nu)^2$ or $(\alpha h\nu)^{1/2}$ vs. $h\nu$ (assuming $E_{ph} << E_g$) provides the bandgap energy of a semiconductor. Fig. 3 allows a direct transition to be identified. As we were unable to determine

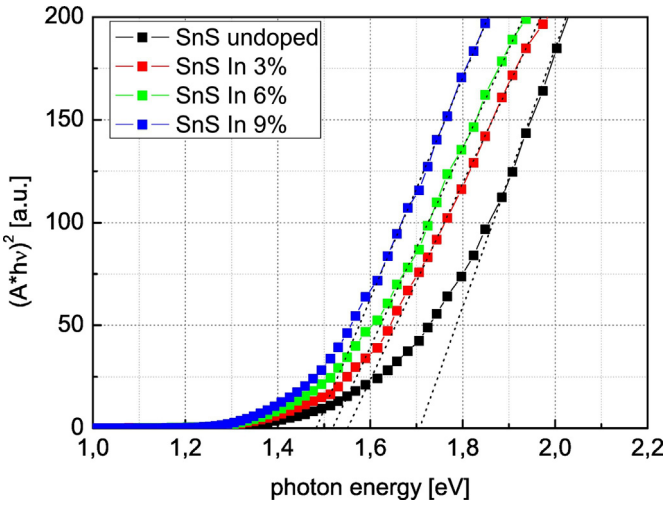

Fig. 3. Plot of $(Ah\nu)^2$ versus photon energy $h\nu$ of SnS films with different In concentrations. An extrapolation of the straight part of the plot is included with dotted lines.

Table 2
Energies obtained from extrapolating the straight part of the appropriate plots for direct and indirect transitions for SnS films with different In concentrations.

[In]/[Sn] ratio (%)	Direct transition energy (eV)	Indirect transition energy (eV)
0	1,71 ± 0,13	1.05 ± 0,03
3	1,55 ± 0,09	1.04 ± 0,03
6	1,52 ± 0,11	1.06 ± 0,04
9	1,48 ± 0,09	1.09 ± 0,04

the thickness (d) of the layers precisely, the absorption coefficient (α) is replaced here by the A = αd. Based on a previous work on spray deposited SnS.

The direct bandgap energies depend on the In concentration in the sprayed solution, and decrease from 1,71 eV for the undoped film to 1.48 eV for the film prepared with 9% concentration of In (Table 2). This is consistent with the available data on SnS thin films, which mostly report it as a direct bandgap semiconductor with bandgap energies of around 1,5 eV [10,12,17]. This effect has already been observed [12] and explained by effective bandgap narrowing due to increased shallow acceptor concentration and the formation of a defect intermediate energy band close to the valence band. However, this effect starts to be significant when carrier concentrations approach atomic concentrations and has been observed e.g. in heavily doped ZnO [18]. This is not the case for the investigated SnS samples, as their conductivity did not indicate such high carrier concentrations. The other reason for the lower bandgap in the In-doped SnS is twofold. The band structure of the material can change with the addition of In, which will directly change the bandgap energy. However, the XRD data show the same crystal structure of the material in all the samples. This also implies no significant changes in the band structure. It can be noted that the fitting was made here for energies above 1,6 eV. The $(Ah\nu)^{1/2}$ vs. $h\nu$ plot and a fitting made for lower energies reveal an indirect transition of around 1.05 eV, independent of In concentration (Fig. 4). This agrees well with the theoretical calculations of the SnS band structure, which indicate an indirect bandgap energy of 1,07 eV [6].

3.3. Photoluminescence

Photoluminescence is a widely used method to study defects in semiconductors by analysing radiative recombination processes. Fig. 5a shows a PL spectrum of an undoped SnS thin film measured at 10 K. The spectrum is a superposition of two radiative processes,

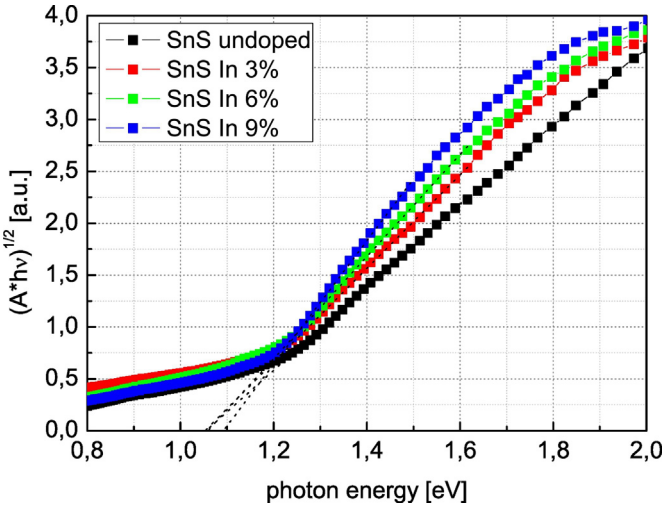

Fig. 4. Plot of $(Ah\nu)^{1/2}$ versus photon energy $h\nu$ of SnS films with different In concentrations. An extrapolation of the straight part of the plot is included with the dotted lines.

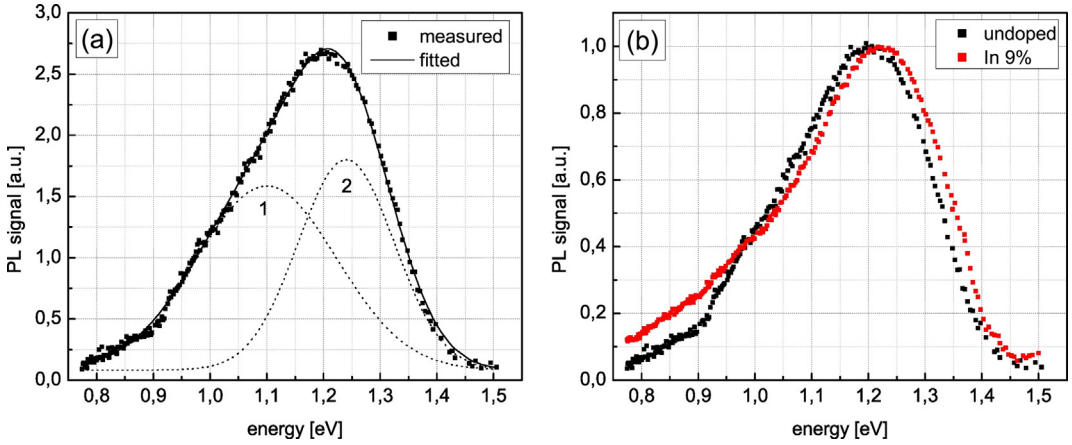

Fig. 5. (a) A photoluminescence spectrum of an undoped SnS thin film measured at 10 K. Fitting with two Gaussian functions (1 and 2) is included on the graph. (b) Comparison of PL spectra for an undoped SnS layer and an SnS layer prepared with 9% indium in the solution. The spectra are normalised to unity for clarity.

labelled on Fig. 5a as (1) and (2). Fittings made with two Gaussian distributions give energies of observed radiative processes of around $E_A = 1{,}1$ eV and $E_B = 1{,}24$ eV. The In doping does not change the shape of the PL spectrum significantly (Fig. 5b). A 20 meV shift is observed in the sample with 9% of indium; but in the other cases the change was negligible. There is also a change in the low-energy part, but looking at all the samples, these changes did not follow any systematic trend.

The luminescence intensity I_{PL} follows a power-law dependence on the excitation intensity I_{ex}:

$$I_{PL} = A^* I_{ex}{}^{\gamma} \tag{4}$$

where A and γ are constants. It has been found that the type of transition can be identified by the value of γ, with $\gamma < 1$ indicating a donor to acceptor transition, $\gamma = 1$ - free to bound transitions and $1 < \gamma < 2$ - exciton-like transitions [19]. Fig. 6 shows the PL intensity dependence on the excitation power. Fitting with a power-law dependence (Eq. 4) give the parameter $\gamma = 0{,}54 \pm 0{,}08$, which points to donor to acceptor (DA) transitions.

To determine the defect thermal activation energies, temperature-dependent measurements were performed. With increased temperature, the process of thermal emission from defect level to the nearest band becomes more probable than recombination, and the intensity of PL decreases. The activation energy of a defect can then be calculated from quenching of the PL signal according to [20]:

$$PL \propto \frac{1}{1 + T^{3/2} \sum_{i=1} a_i e^{-eE_{ai}/k_B T}} \tag{5}$$

where a_i is constant including a capture cross-section, E_{ai} is the thermal activation energy of a defect, and k_B is the Boltzmann constant. The quenching of two identified DA transitions is shown on Fig. 7 together with the PL spectra at different temperatures.

The fittings made using Eq. (4) gave in both cases one thermal activation energy, which is the activation energy of a shallower defect taking part in the donor-acceptor recombination process. We obtained the following values of $E_{a1} = 85 \pm 11$ meV and $E_{a2} = 93 \pm 13$ meV. Taking into account the quality of the PL spectra and the quality of the fit itself, we conclude that in both transitions, one of the defect levels taking part in the recombination process is the same and has a thermal activation energy of 89 ± 12 meV. The second defect must introduce, in both cases, a deep level, because the sum of the activation energy and the transition energies is much lower than the bandgap value.

3.4. Conductivity measurements

The applicability of a material as an absorber in a solar cell requires not only good optical properties but also appropriate electrical conductivity. Fig. 8 presents the electrical conductivity dependence on

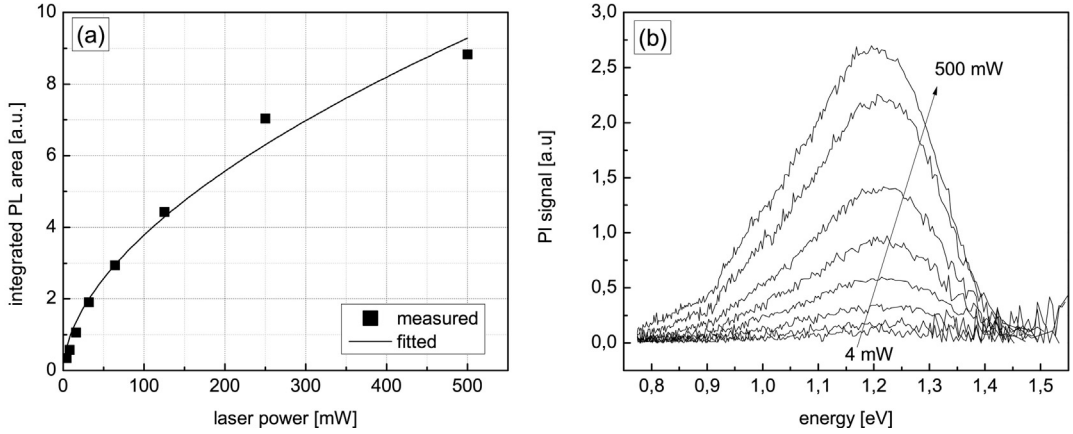

Fig. 6. (a) Integrated area of Pl spectra measured at 10 K as a function of laser power. Fitting was made with a power-law dependence (Eq. 4) and is included on the graph. (b) Complete PL spectra in the 4–500 mW laser power range.

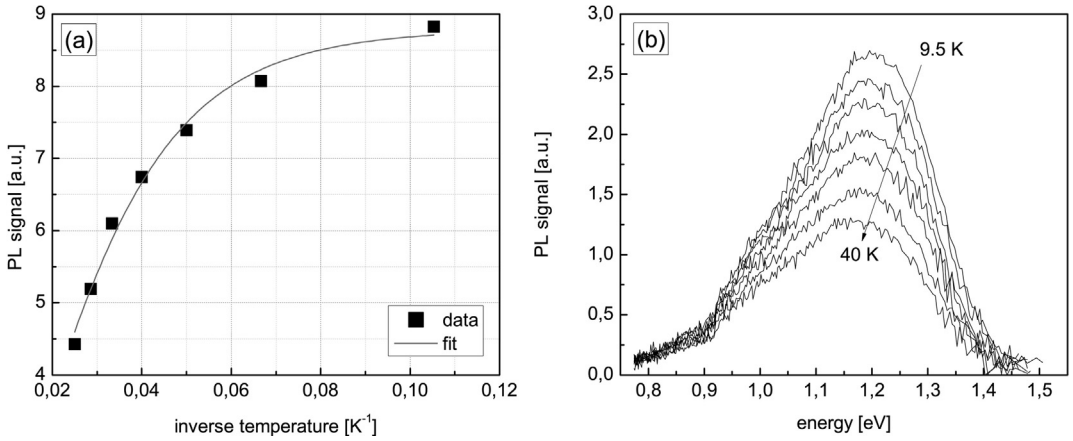

Fig. 7. (a) Quenching of PL intensity for two observed donor-acceptor transitions with increasing temperature. Fittings made using Eq. 5 are included on the graph. (b) Complete PL spectra recorded over the 9,5–40 K temperature range.

temperature for all investigated films. For temperatures above 200 K, the conductivity is thermally activated and follows an exponential dependence on (1/T). Thus, the linear fitting to the logarithm of conductivity versus (1/T) provides the activation energy (E_{act}) of conductivity, which for a p-type semiconductor is the energy distance from the acceptor level (E_A) and the valence band $E_{act} = E_V$-E_A. The undoped SnS had an activation energy of 164 ± 2 meV and did change significantly, except for the sample with 9% In concentration, where a value of 145 ± 2 meV was obtained. Additionally, a slightly lower (160 ± 2 meV) activation energy in a layer with 6% In concentration may point to the decreasing dependence of activation energy on In concentration. Taking into account the fact that the energy of a direct bandgap depends on the amount of indium in the solution, this might mean that the energy position of the acceptor level responsible for the conductivity also changes when In is introduced.

The conductivity at room temperature increases with of the amount of indium by a factor of 1,78 between an undoped SnS film and one doped with 9% of In. This might be the result of decreased activation energy. The observable decrease of activation energies from 164 meV to 145 meV should itself give an increase of conductivity by a factor of 2,1 ± 0.4.

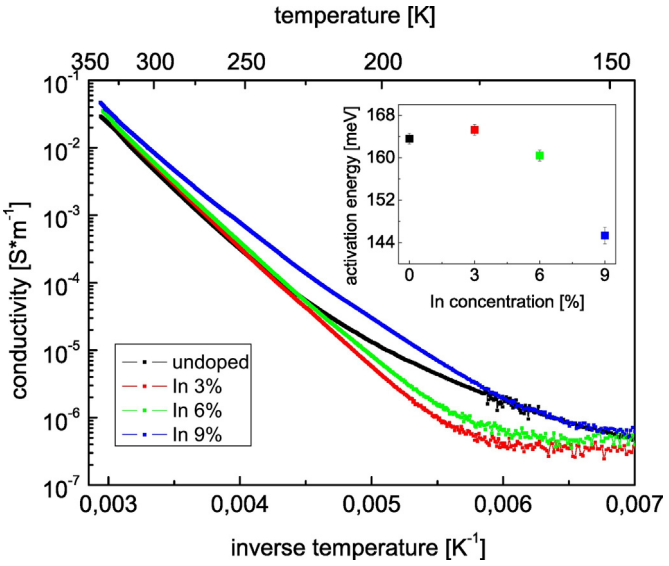

Fig. 8. Electrical conductivity dependence on temperature for investigated series of thin films. The linear fittings were made over the same 250–330 K temperature range for all the samples, providing activation energies included in the inset.

4. Conclusions

We have presented an opto-electrical study of In-doped SnS thin films made by spray pyrolysis. XRD analysis revealed an orthorhombic structure with a (111) dominant peak. AFM imaging shows that the films consist of longitudinal grains. The In doping slightly increases the roughness of the surface as well as the average size of the grains, while the crystallite size remains constant. The material has an indirect bandgap with energy of around 1.05 eV, independent of In concentration. However, the absorption is dominated by the direct transition with energies decreasing with increasing amounts of indium from 1,71 eV to 1,48 eV. The PL study revealed two donors to acceptor transitions, independent of the In concentration. In both transitions, one of the defect levels taking part in the recombination process is commonly characterised by thermal activation energy of around 90 meV. However, we could not judge whether the defect was a donor or an acceptor. The conductivity measurements show thermally activated conductivity with activation energies inversely proportional to In concentration in the 145–162 meV range. This decrease of activation energy directly results in the higher conductivity of the investigated thin films.

Acknowledgments

This work was supported by the Ministerio de Economía y Competitividad (ENE2016-77798-C4-2-R) and Generalitat Valenciana (Prometeus 2014/044).

References

[1] P. Jackson, D. Hariskos, R. Wuerz, O. Kiowski, A. Bauer, T.M. Friedlmeier, M. Powalla, Properties of Cu(In,Ga)Se_2 solar cells with new record efficiencies up to 21.7%, Phys. Stat. Sol. (2015) 28–31 (RRL) 9 http://dx.doi.org/10.1002/pssr.201409520.
[2] M. Gloeckler, I. Sankin, Z. Zhao, CdTe solar cells at the threshold to 20% efficiency, IEEE J. Photovoltaics 3 (2013) 1389–1393, http://dx.doi.org/10.1109/JPHOTOV.2013.2278661.
[3] K.T. Ramakrishna Reddy, N. Koteswara Reddy, R.W. Miles, Photovoltaic properties of SnS based solar cells, Sol. Energy Mater. Sol. Cells 90 (2006) 3041–3046, http://dx.doi.org/10.1016/j.solmat.2006.06.012.
[4] L. Yu, S. Lany, R. Kykyneshi, V. Jieratum, R. Ravichandran, B. Pelatt, E. Altschul, H.A.S. Platt, J.F. Wager, D. Keszler, A. Zunger, Iron chalcogenide photovoltaic absorbers, Adv. Energy Mater. 1 (2011) 748–753, http://dx.doi.org/10.1002/aenm.201100351.
[5] A. Ashour, The physical characteristics of Cu_2S/CdS thin-film solar cell, J. Optoelectron. Adv. Mater. 8 (2006) 1447–1451.
[6] J. Vidal, S. Lany, M. d'Avezac, A. Zunger, A. Zakutayev, J. Francis, J. Tate, Band-structure, optical properties, and defect physics of the photovoltaic semiconductor SnS, Appl. Phys. Lett. 100 (032104) (2012)http://dx.doi.org/10.1063/1.3675880.
[7] W. Shockley, H.J. Queisser, Detailed balance limit of efficiency of p-n junction solar cells, J. Appl. Phys. 32 (1961) 510–519, http://dx.doi.org/10.1063/1.1736034.

[8] R. Jaramillo, V. Steinmann, C. Yang, K. Hartman, R. Chakraborty, J.R. Poindexter, M. Lizet Castillo, R. Gordon, T. Buonassisi, Making record-efficiency SnS solar cells by thermal evaporation and atomic layer deposition, J. Vis. Exp. 99 (2015) 5–22, http://dx.doi.org/10.3791/52705.
[9] N. Koteswara Reddy, K.T. Ramakrishna Reddy, Growth of polycrystalline SnS films by spray pyrolysis, Thin Solid Films 325 (1–2) (1998) 4–6, http://dx.doi.org/10.1016/S0040-6090(98)00431-3.
[10] T. Sall, M. Mollar, B. Marí, Substrate influences on the properties of SnS thin films deposited by chemical spray pyrolysis technique for photovoltāic applications, J. Mater. Sci. 51 (2016) 7607–7613, http://dx.doi.org/10.1007/s10853-016-0039-9.
[11] B.D. Malone, A. Galibc, E. Kaxirasad, First principles study of point defects in SnS, Phys. Chem. Chem. Phys. 16 (2014) 26176–26183, http://dx.doi.org/10.1039/c4cp03010a.
[12] K.S. Kumar, C. Manoharan, S. Dhanapandian, A.G. Manohari, T. Mahalingam, Effect of indium incorporation on properties of SnS thin films prepared by spray pyrolysis, Optik-Int. J. Light Electron Opt. 125 (2014) 3996–4000, http://dx.doi.org/10.1016/j.ijleo.2014.01.144.
[13] H. Chaki Sunil, D. Chaudhary Mahesh, M.P. Deshpande, Effect of indium and antimony doping in SnS single crystals, Mater. Res. Bull. 63 (2015) 173–180, http://dx.doi.org/10.1016/j.materresbull.2014.12.013.
[14] T.G. Hibbert, M.F. Mahon, K.C. Molloy, L.S. Price, I.P. Parkin, Deposition of tin sulfide thin films from novel, volatile (fluoroalkythiolato) tin (IV) precursors, J. Mater. Chem. 11 (2001) 469–473.
[15] T. Sall, B.M. Soucase, M. Mollar, J.A. Sans, SnS thin films prepared by chemical spray pyrolysis at different substrate temperatures for photovoltaic applications, J. Electron. Mater. 46 (2017) 1714–1719.
[16] J.I. Langford, A.J.C. Wilson, Scherrer after sixty years: a survey and some new results in the determination of crystallite size, J. Appl. Crystallogr. 11 (1978) 102–113.
[17] J.A. Andrade-Arvizu, M. Courel-Piedrahita, O. Vigil-Galán, SnS-based thin film solar cells: perspectives over the last 25 years, J. Mater. Sci. Mater. Electron. 26 (2015) 4541–4556.
[18] C.E. Kim, P. Moon, S.Y. Kim, J.-M. Myoung, H.W. Jang, J.S. Bang, I.G. Yun, Effect of carrier concentration on optical bandgap shift in ZnO: Ga thin films, Thin Solid Films 518 (2010) 6304–6307.
[19] J.I. Pankove, Optical Processes in Semiconductors, Dover Publications, New York, 1975.
[20] H. Shibata, Negative thermal quenching curves in photoluminescence of solids, Jpn. J. Appl. Phys. 37 (1998) 550–553.